

MEASUREMENTS OF SOLAR IRRADIANCE AND EFFECTIVE TEMPERATURE AS A PROBE OF SOLAR INTERIOR MAGNETIC FIELDS

L. H. LI^{1,2} AND S. SOFIA

Department of Astronomy, Yale University, P.O. Box 208101, New Haven, CT 06520-8101

Draft version December 2, 2024

ABSTRACT

We argue that a variety of solar data suggest that the activity-cycle timescale variability of the total irradiance is produced by structural adjustments of the solar interior. On the assumption that these adjustments are induced by variations of internal magnetic fields, we use measurements of the total irradiance and effective temperature over the period from 1978 to 1992 to infer the magnitude and location of the magnetic field. Based on an updated stellar evolution model with magnetic fields taken into account, we find that the observations can be explained by fields whose peak values range from 120k to 2.3k gauss, located in the convection zone at depths ranging from $r = 0.950R_{\odot}$ to $0.997R_{\odot}$, respectively. The corresponding maximal radius changes range from 19 to 3 km, and $W = d \ln R / d \ln L$ from 0.03 to 0.006. All these predictions are consistent with helioseismology and recent measurements carried out by the MDI experiment on SOHO.

Subject headings: Sun: interior — Sun: magnetic fields

1. INTRODUCTION

Direct satellite measurements of total solar irradiance (Willson & Hudson 1991; Fröhlich & Lean 1998) show that it varies almost in phase with the solar activity cycle and that its variation amplitude $\Delta \ln S$ is about 0.1%. Although the most common explanation provided for this change involves the effect of magnetic regions and network (superposed to an otherwise constant solar photosphere), an alternative explanation is that the cyclic variation is primarily due to structural changes of the solar interior. Two arguments support this second possibility. First, direct measurements of the spectrum of p-mode oscillations show variations (Libbrecht & Woodard 1990) that can be best explained in terms of structural changes (i.e. changes in pressure, density, radius, etc) (Lydon et al 1996; Antia et al 2000; Balmforth et al 1996). Second, the measurements of the “effective temperature” by Gray and Livingston (1997) also show a variation nearly in phase with the solar cycle. This variation is obtained by monitoring the neutral carbon $\lambda 5380$ line in the solar flux spectrum. They present several arguments supporting their contention that what they measured was the gas temperature in the deep photosphere, free from the influence of sunspots, faculae and small scale magnetic flux tubes. Their main argument rests on their simultaneous monitoring of C I $\lambda 5380$, Fe I $\lambda 5379$ and Ti II $\lambda 5381$. They used the ratios of spectral line depths, C I $\lambda 5380$ to Fe I $\lambda 5379$ and to Ti II $\lambda 5381$ as the temperature indicators. Since these three lines have different excitation potentials (1.57 eV for Ti II $\lambda 5381$, 3.69 eV for Fe I $\lambda 5379$, and 7.68 eV for C I $\lambda 5380$), the consistency of the the results for the two line depth ratios shows that the temperature indicators are free from influence of variations of faculae and small scale magnetic flux tubes, which would be expected to affect each line in a different way. See Gray & Livingston (1997a,b) for the entire

discussion. In order for the gas temperature to change, the energy flow from the interior must also change. Structural adjustment will be able to accomplish this. Since $\Delta \ln R$ is very small (Emilio et al 2000),

$$\Delta \ln L \approx 4 \Delta \ln T. \quad (1)$$

The temperature change measured by Gray and Livingston (1997) is 1.5 ± 0.2 K, which corresponds to $\Delta \ln T \sim 0.025\%$ and $\Delta \ln L \sim 0.1\%$. This is approximately the entire variation of the total irradiance.

The most obvious way the solar structure may change is in response to variations of the internal magnetic field during the dynamo build-up and decay. In order to compute this effect, we introduce magnetic variables as new stellar structure variables (Lydon & Sofia 1995) in addition to the conventional ones (Guenther et al 1992). Since magnetic field is not a scalar, we have to use at least two variables to describe it: the magnetic energy density χ (Lydon & Sofia 1995) and the ratio of the magnetic pressure to the magnetic energy, $\gamma - 1$ (Endal et al 1985). This method was developed by Lydon and Sofia in 1995, in which γ was treated as a parameter, and it was subsequently applied by Lydon, Guenther and Sofia (1996) to explain the observed variation of solar p-mode oscillations with the solar cycle (Libbrecht & Woodard 1990). Here we want to update this method by: (i) treating both χ and γ as new structure variables, as done for χ in Lydon and Sofia (1995), (ii) taking into account the influence of magnetic fields on radiative opacities, (iii) taking into account all time-dependent contributions to the equations of stellar structure since we want to treat short time scales, (iv) modifying the radiative loss assumption of a convective element as will be discussed in section 3, (v) updating the code by using the new version of the stellar evolution code with rotation (YREC7) and (vi) removing the perfect gas approximation assumed in calculating some first- and second-order derivatives associated with magnetic fields.

¹also at Purple Mountain Observatory, Chinese Academy of Sciences

²also at National Astronomical Observatories, Chinese Academy of Sciences

Because luminosity, radius and temperature variations are sensitive to the location, intensity, orientation, and distribution of the perturbation magnetic field $B = (8\pi\chi\rho)^{1/2}$ (where ρ is the gas density), we can use the measured yearly-averaged irradiance, temperature and radius variations to determine the solar interior magnetic field as a function of mass and time.

2. SOLAR IRRADIANCE AND EFFECTIVE TEMPERATURE RECORDS

Space-based solar irradiance measurements have been reviewed by Fröhlich and Lean (1998), and a composite solar irradiance record for the period from 1978 to the present can be downloaded from the website <http://www.ngdc.noaa.gov/>. In our magnetic perturbation model calculations we use one year as the timestep, so we sum the measured solar irradiance values for each year and then divide the sum by the total number of data points to obtain the yearly mean of total solar irradiance, as shown in Figure 1. The standard variances range from 0.1 Wm^{-2} to 0.5 Wm^{-2} .

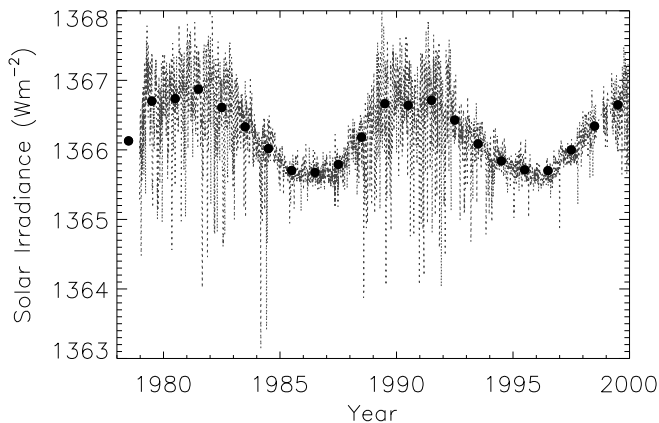


FIG. 1.— A composite solar irradiance record from the end of 1978 to the present (Fröhlich & Lean 1998) and the yearly mean of solar irradiance.

The spectroscopic temperature variations of the sun measured by Gray and Livingston (1997) over the period from 1978 to 1992, are shown in Figure 2, which is reproduced from their Figure 9. The points are the yearly means, and the zero point is chosen arbitrarily.

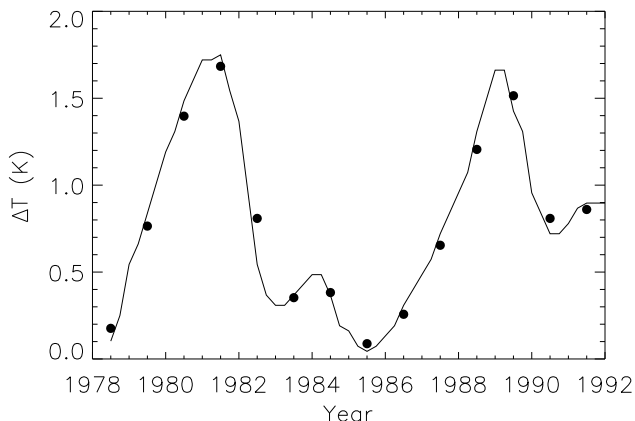


FIG. 2.— The measured solar photospheric temperature variations from 1978 to 1992 (Gray & Livingston 1997b) and the yearly mean.

3. METHOD

3.1. Definition of variables

Standard solar models (SSM) use pressure, temperature, radius and luminosity as the structure variables and use the mass M_r interior to a radius r as the independent variable. In order to self-consistently take into account magnetic effects, Lydon and Sofia (1995) introduced two new magnetic structure variables to model the sun: the magnetic energy per unit mass χ , and the effective ratio of specific heats for the magnetic perturbation γ . The former describes the magnetic perturbation strength, and the latter describes the tensor feature of the magnetic pressure. In general, the determination of χ and γ requires a comprehensive understanding of turbulent dynamics in the solar convective zone (Brummell et al 1995), an undertaking that is impractical at present. Therefore, we take χ and γ as free parameters (functions) that need to be determined at this stage instead of using their governing equations to determine them.

Our aim is to use the measured solar irradiance and effective temperature variations given in Figures 1 and 2 to determine $\chi(M_D, t)$ and $\gamma(M_D, t)$ as a function of the mass depth M_D and time t so that we can obtain a solar interior magnetic field $B(M_D, t) = (8\pi\chi\rho)^{1/2}$. The mass depth M_D is defined as

$$M_D = \log_{10}(1 - M_r/M_\odot) \quad (2)$$

which replaces the mass variable M_r when we want to express the location, orientation and form of all magnetic perturbations.

For our purpose we can use the toroidal (B_t) and poloidal (B_p) components to express a magnetic field vector $\vec{B} = (B_t, B_p)$. For the sake of convenience, we introduce two new variables to replace these two components. The first is the magnetic energy density variable χ :

$$\chi = (B^2/8\pi)/\rho \quad (3)$$

where $B = (B_t^2 + B_p^2)^{1/2}$ is the magnitude of the magnetic field vector. The second is the magnetic field direction variable γ , defined as

$$\gamma = (2B_t^2 + B_p^2)/B^2. \quad (4)$$

The magnetic pressure P_χ can be expressed by new magnetic variables χ and γ as follows

$$P_\chi = (\gamma - 1)\chi\rho. \quad (5)$$

Obviously, $1 \leq \gamma \leq 2$ depends on the field geometry. The magnetic pressure component parallel to the field line is zero, so $\gamma = 1$, while the one perpendicular to the field line reaches the maximum value of possible magnetic pressure with fixed strength B , leading to $\gamma = 2$.

3.2. Consequencies on the equations of stellar structure

The continuum equation remains intact. The hydrostatic equation is replaced by the equation of motion with the Lorentz force

$$\rho \frac{d^2 \vec{r}}{dt^2} = -\nabla P - \frac{GM_r}{r^2} \rho \hat{r} + \frac{1}{4\pi} (\nabla \times \vec{B}) \times \vec{B}.$$

The radial component is

$$\rho \frac{d^2 r}{dt^2} = -\frac{dP}{dr} - \frac{GM_r}{r^2} \rho - \frac{dP_\chi}{dr},$$

where the direction of \vec{B} has been parameterized as γ , $\gamma = 1$ so that $dP_\chi/dr = 0$ when \vec{B} is parallel to \hat{r} , $\gamma = 2$ so that $dP_\chi/dr = d(\chi\rho)/dr$ when \vec{B} is perpendicular to \hat{r} . Defining

$$P_T = P + P_\chi$$

as the total pressure, the equation of radial motion looks like a hydrostatic equilibrium equation

$$\frac{\partial P_T}{\partial M_r} = -\frac{GM_r}{4\pi r^4} - \frac{1}{4\pi r^2} \frac{d^2 r}{dt^2} \quad (6)$$

The last term represents the inertial force. Since

$$\rho = \rho(P_T, T, \chi, \gamma)$$

the equation of state becomes

$$\frac{d\rho}{\rho} = \alpha \frac{dP_T}{P_T} - \delta \frac{dT}{T} - \nu \frac{d\chi}{\chi} - \nu' \frac{d\gamma}{\gamma}$$

where

$$\begin{aligned} \alpha &= \frac{\partial \ln \rho}{\partial \ln P_T} \text{ at constant } T, \chi, \gamma \\ \delta &= -\frac{\partial \ln \rho}{\partial \ln T} \text{ at constant } P_T, \chi, \gamma \\ \nu &= -\frac{\partial \ln \rho}{\partial \ln \chi} \text{ at constant } P_T, T, \gamma \\ \nu' &= -\frac{\partial \ln \rho}{\partial \ln \gamma} \text{ at constant } P_T, T, \chi \end{aligned}$$

The energy conservation equation becomes

$$\frac{\partial L}{\partial M_r} = \epsilon - T \frac{dS_T}{dt} - \frac{1}{\rho} \frac{du}{dt}. \quad (7)$$

Here

$$\begin{aligned} TdS_T &= dQ_T = dU + PdV + d\chi \\ &= dU_T + P_T dV - (\gamma - 1)(\chi/V)dV \\ &= c_p dT - \frac{\delta}{\rho} dP_T + \left(1 + \frac{P_T \delta \nu}{\rho \alpha \chi}\right) d\chi + \frac{P_T \delta \nu'}{\rho \alpha \gamma} d\gamma \end{aligned} \quad (8)$$

is the generalized first law of thermodynamics, in which $U_T = U + \chi$ and $S_T = S + \chi/T$. If we treat γ as a parameter, $d\gamma = 0$, equation (8) reduces to equation (75) in Lydon & Sofia (1995). $u = aT^4$ is the radiation energy density, du/dt is the time derivative term that should appear in the full energy conservation equation

$$\frac{\partial u}{\partial t} + \nabla \cdot \vec{F} = \rho(\epsilon - TdS_T/dt)$$

$\vec{F} = u\vec{v}$ is the radiation energy flux vector, in which \vec{v} is the photon diffusion velocity.

The equation of transport of energy by radiation

$$\frac{\partial T}{\partial M_r} = -\frac{3}{64\pi^2 ac} \frac{\kappa l}{r^4 T^3} \quad (9)$$

does not change in form, but the magnetic field may affect the opacity coefficient κ . A magnetic field affects the absorption processes that are associated with free electrons, such as electron scattering absorption κ_{sc} and free-free transition absorption κ_{ff} . We can estimate this effect in terms of the mean free paths without and with magnetic field, l_0 and l_B

$$\kappa_{e0}/\kappa_{eB} \propto (l_B/l_0)^2 \approx 1 + \frac{1}{4}(\gamma - 1)\tau_e^2 \Omega_e^2 \quad (10)$$

Here $1/\tau_e$ is the collision frequency between electrons, $\kappa_e = \kappa_{sc} + \kappa_{ff}$ is the absorption component that will be

affected by magnetic field, Ω_e is the electron cyclotron frequency.

The equation of transport of energy by convection

$$\frac{\partial T}{\partial M_r} = -\frac{T}{P_T} \frac{GM_r}{4\pi r^4} \nabla \quad (11)$$

does not change in form either, but the convection temperature gradient with a magnetic field is different than that without magnetic field.

$$\nabla = \nabla_{ad} + \begin{cases} (y/V\gamma_0^2 C)(1 + y/V) & \text{for } \chi = 0 \\ (y'/V'\gamma_0^2 C)(1 + y'/V') - A_m & \text{for } \chi \neq 0 \end{cases} \quad (12)$$

where

$$\begin{aligned} V &= 1/[\gamma_0 C^{1/2}(\nabla_{rad} - \nabla_{ad})^{1/2}] \\ 0 &= 2Ay^3 + Vy^2 + V^2y - V \end{aligned}$$

when $\chi = 0$ and

$$\begin{aligned} V' &= 1/[\gamma_0 C^{1/2}(\nabla_{rad} - \nabla_{ad})^{1/2} + A_m] \\ 0 &= 2Ay'^3 + V'y'^2 + V'^2y' - V' \end{aligned}$$

when $\chi \neq 0$, in which the initial χ of the convection element is assumed to remain frozen in the surrounding material. We have defined

$$A_m \equiv f'[(\nu/\alpha)\nabla_\chi + (\nu'/\alpha)\nabla_\chi]\nabla_{ad}, \quad (13)$$

where f' is a dimensionless parameter that determines the influence of magnetic field on radiative loss of a convective element. In Lydon and Sofia (1995), f' is assumed to be 1 implicitly. Consequently, the effective temperature of such a solar model varies in antiphase with solar activity cycle, contrary to the observed trend by Gray and Livingston (1997b). We find that $f' = 3$ can match the observation very well. Definitions of adiabatic gradient ∇_{ad} and specific heats, c_p and c_v , are also different from the conventional ones, but similar to the definition of α or δ , see Lydon and Sofia (1995), in which we can also find the definitions for ∇_{rad} , A , C , γ_0 and ∇_χ . The definition of ∇_γ is similar to that of ∇_χ .

3.3. Numerical implementation

In order to follow the yearly variations of solar global parameters by using a stellar evolution code, we have to use one year as the timestep. Consequently, we have to make use of a precise code that allows a timestep at least as short as one year. For example, because L_\odot has increased about 30% during the lifetime of the sun, the relative mean rate of change is about 10^{-10} per year. To achieve such a high precision is a challenge. Fortunately, Yale stellar evolution code with rotation (YREC) meets this need, as shown before (Lydon & Sofia 1995). We follow Lydon and Sofia (1995) by modifying YREC7, a new version released in May 1999, in order to accommodate the magnetic effects described above. The reason why YREC permits a small timestep and achieves such a high numerical precision traces back to the fact that it uses analytical formulae (Prather 1976) rather than numerical methods to calculate the partial derivatives of the differential equations of stellar structure with respect to the dependent variables, which are required for the widely used linearization method to calculate stellar model corrections due to evolution.

YREC solves the linearized equations of stellar evolution in one dimension (rotation is represented in an oblate coordinate system to maintain the 1-D nature of the code). The pressure, temperature, radius, and luminosity are solved at a given time, as a function of mass. A set of finite difference equations relate the pressure, temperature, radius, and luminosity, as a function of mass and time, at each shell in the model. The energy generation rate, the mean molecular weight, the density and the opacity are calculated separately. The reaction rates of all the important nuclear reactions (pp chains, CNO cycles, triple-alpha, and some light element reactions) are determined from the known nuclear cross sections. By solving the network of reactions the program determines both the nuclear photon and neutrino luminosity and the evolution of the elements involved in the reactions for each shell. The equation of state routines calculate the density and other thermodynamic variables. Once the new composition of elements is determined, the mean molecular weight and the opacities are calculated. Tables of opacity, a function of temperature, density and chemical composition are interpolated to obtain the opacity in each shell of the model. The equation of state can be calculated empirically using an approximate formula relating density to the pressure and temperature, which takes into account the degree of ionization of hydrogen and helium, or it can be obtained by interpolating a set of tables.

In order to accommodate the various magnetic effects described above, we must first write a routine to specify χ , γ . We assume $\chi = \chi_m(t)F(M_D)$. The maximum χ , $\chi_m(t)$, is to be determined from solar activity indices. The yearly-averaged sunspot number R_Z is the most widely used solar activity index. We find that if the maximum magnetic field in the solar interior B_m can be related to R_Z as follows,

$$B_m = B_0\{A + [1 + \log_{10}(1 + R_Z)]^5\}, \quad (14)$$

and we can make a good fit to the measured cyclic variations of irradiance and effective temperature by adjusting B_0 and A . B_m determines χ_m . $F(M_D)$ specifies the distribution of χ and is to be determined by fitting the measured irradiance and effective temperature variations. $F(M_D)$ has infinite degrees of freedom and thus cannot be determined uniquely by the above described observational information of finite degrees of freedom. However, we can use the existing data to probe the location of the solar interior magnetic field with a localized distribution

$$F(M_D; M_{Dc}, \sigma) = \exp[-\frac{1}{2}(M_D - M_{Dc})^2/\sigma^2], \quad (15)$$

where M_{Dc} specifies the location and σ specifies its width. We fix γ , or use

$$\gamma(M_D) = 1 + (B/B_m)^{1/5}(R_Z/200) \quad (16)$$

to express the spatial and temporal variations of the direction of magnetic fields, which implies that the more intense the magnetic field the larger its toroidal component.

We do not consider the influence of magnetic fields on the energy generation rate in this paper, since the magnetic fields that cause the solar activity cycle are believed to exist outside of the solar core where the thermonuclear reactions occur.

Magnetic fields affect the equation of state, which is called the β -effect (Endal et al 1985) since it can be

described by redefining β , the ratio of the gas pressure to the total pressure when magnetic fields are present,

$$\beta = 1 - \frac{\frac{1}{3}aT^4}{P_T} - \frac{(\gamma - 1)\chi\rho}{P_T}, \quad (17)$$

where a is the radiation constant. Using this definition, the density of a gas is still determined by

$$\beta P_T = \mathcal{R}\rho T(1 + E)/\mu_a, \quad (18)$$

where \mathcal{R} is the gas constant, E is the number of free electrons per nucleus and it is determined by solving the Saha equation, μ_a is the mean atomic weight per atom (Prather 1976). E also depends on β . In the standard case, since $\chi = 0$, β does not depend on ρ . But in the nonstandard case discussed in this paper, β depends on ρ . Consequently, not only ρ , but also its first derivatives α , δ , ν , and ν' , and its second derivatives with respect to T and P_T all need to be calculated by iteration, which is tedious. In the original implementation of this method by Lydon and Sofia (1995), ρ is obtained by iteration, but its first derivatives are calculated by using the counterpart of the adjacent point as the initial guess without iteration in calculating the first derivatives of E , the second derivatives are approximated by assuming the gas to be perfect, which needs no iteration. In this code upgrade, we modify the equation of state routine so that we can accurately calculate all these thermodynamic variables by iteration. This improves the numerical precision, but does not make any qualitative difference. The qualitative difference comes from f' , which parameterizes the influence of magnetic fields on radiative loss of a convection element, as pointed out above. Besides, ∇_χ and ∇_γ are calculated by numerical derivatives, and so are those time derivatives which appear in the equations of stellar structure.

The influence of magnetic fields on the radiative opacity can only be treated approximately since we use only opacity tables. We assume that we can decompose the total opacity coefficient κ into two parts: $\kappa = \kappa_e + \kappa_1$ since κ_{sc} and κ_{ff} do not or only weakly depend on frequency before making the so-called Rosseland mean. We use the opacity subroutine provided by YREC7 to calculate κ and use equations (17.2) and (17.5) in Kippenhahn and Weigert (1990) to calculate κ_e . The opacity corrected by magnetic fields, κ' , can be expressed approximately as follows due to equation (10)

$$\kappa' = \kappa - \kappa_e \frac{(\gamma - 1)\tau_e^2 \Omega_e^2}{4 + (\gamma - 1)\tau_e^2 \Omega_e^2} \quad (19)$$

The approximation originates from the fact that the absorption due to free-free transitions depends on frequency as $\kappa_\nu \propto \nu^{-3}$. We add a subroutine to calculate this magnetic correction to the opacity, whose influence turns out to be negligible.

The temperature gradient routine is modified to accommodate A_m defined in equation (13). In the original implementation by Lydon and Sofia (1995),

$$A_m \equiv (\nu/\alpha)\nabla_\chi \nabla_{ad}. \quad (20)$$

When $f' = 1$ and γ is fixed equation (13) reduces to this expression. It is $f' = 3$ it reverses the variation trend of effective temperature calculated by using $f' = 1$. Again, f' parameterizes the influence of magnetic fields on the radiative loss of a convective element.

We do not redistribute the mass grid points, nor do we predict stellar structure variables for the next time step, when the timestep is smaller than a solar cycle period, since these operations will generate an error much larger than 10^{-10} per year for luminosity. All convergence criteria for iteration are tightened by requiring the relative error to be no larger than 10^{-16} or so. In this modified code, the matching point is at $M_D \approx -8.6$.

We find that the magnetic effects are maximized when $\gamma = 2$, so we set $\gamma = 2$ below.

4. CONSTRAINTS ON THE SOLAR INTERIOR MAGNETIC FIELD

At present, it is generally believed that the magnetic field is stored only in the subadiabatically stratified overshoot layer in the form of flux tubes, which may break loose due to kink instabilities when a threshold of 10^5 gauss is exceeded (Caligar et al 1995; Caligar et al 1998). Figure 3 depicts $\nabla - \nabla_{\text{ad}}$ vs M_D , in which the subadiabatically stratified overshoot layer approximately corresponds to the mass depth range: $-1.68 \leq M_D < -1.2$. $M_{\text{Dc}} = -1.68$ corresponds to the base of the convection zone of our model sun. Therefore, the maximum yearly-averaged field strength B_m in the overshoot layer during the solar cycle should be smaller than the threshold. The field with $M_{\text{Dc}} = -1.45$ and $\sigma < 0.2$ can be considered to be confined in the overshoot layer. However, even if the threshold value of B is used, the resultant irradiance and effective temperature variations are negligible.

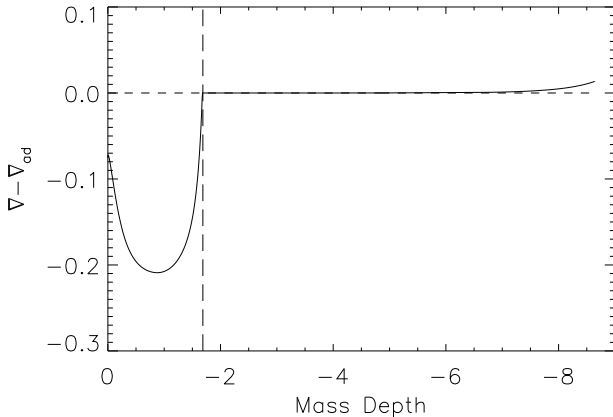


FIG. 3.— The difference between the temperature gradient and the adiabatic gradient as a function of the mass depth in the solar interior. The dashed line marks the location of lower boundary surface of the convection zone.

Only when we abandon this threshold constraint (e.g., using a field larger than 2.6×10^6 gauss), we can get irradiance variations comparable to the observations, in magnitude and phase; however, even then, the effective temperature variation is much smaller and in antiphase with the solar cycle. Besides, the resulting relative radius variation is larger than 0.03%. Since the observations reveal that both irradiance and effective temperature variations are in phase with the solar cycle and the relative radius variation should be much smaller than 0.01% (Emilio et al 2000), we conclude that the magnetic field that gives rise to the observed ΔS and ΔT shown in Figures 1 and 2 cannot be completely confined in the overshoot layer.

We thus investigate the possibility that the magnetic field is located totally within the convection zone. If we

take the field strength as a free parameter, we find that the lower part of the convection zone, $M_{\text{Dc}} > -3.8$ is ruled out because it produces radius changes that are too large. For the next region up, $-7.8 < M_{\text{Dc}} < -3.8$, or $0.950R_{\odot}$ to $0.997R_{\odot}$, B_m ranges from 1.2×10^5 G to 2.3×10^3 G. In this case, the amplitude of the radius changes ranges from 19 to 3 km, and $W = \Delta \ln R / \Delta \ln L$ ranges from 0.03 to 0.006. Setting $\sigma = 0.2$, we find B_0 ranges from 230 G to 4.4 G. $A = 190$ does not change. As a consequence, the location of the field in this entire region is allowed. On the other hand, the outer part, with $M_{\text{Dc}} < -7.8$, is ruled out because the resulting irradiance and effective temperature variations are in antiphase with the solar cycle. In all cases, to produce the observed luminosity and effective temperature variations, the required magnetic field must increase with depth. The resulting W parameter also increases with depth.

In order to pinpoint the location of the required magnetic fields in the allowed region of solar convection zone ($M_{\text{Dc}} \in [-3.8, -7.8]$), we need more information. We obtain the allowed region by using the observational information for solar irradiance and effective temperature cyclic variations and by assuming the corresponding solar radius variation $\Delta \ln R$ to be much smaller than 0.01%. If we have the direct observational information for $\Delta \ln R$ or the W parameter, we can pinpoint the location of solar interior magnetic fields. Since we do not have simultaneous observational information for the radius cyclic variation in the period ranging from 1978 to 1992 we are discussing, we first invoke some physical considerations.

Figure 4 shows the ratio of radiative to adiabatic temperature gradients as a function of mass depth in the sun, from which we can see that the layer with M_D ranging from -4 to -8 is the most unstable convective region. In this layer superstrong plasma turbulence is inevitable since the radiative gradient ∇_{rad} is much larger than the adiabatic temperature gradient ∇_{ad} . Therefore, this may suggest a turbulence generation mechanism for solar magnetic fields. Strong plasma turbulence can generate strong small-scale magnetic fields, which form small magnetic cells with almost random orientation. The residual field of the previous cycle and differential rotation tend to align and bundle these random magnetic “needles” to form flux tubes.

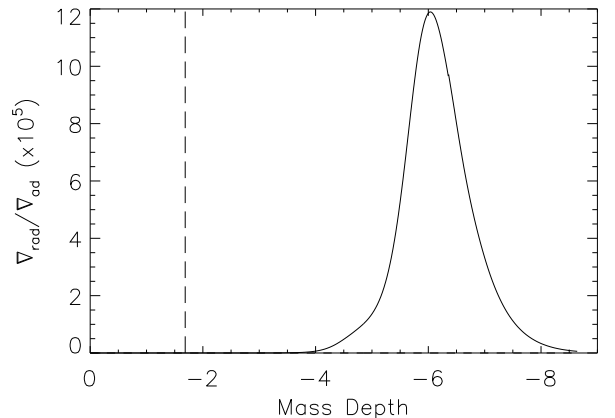


FIG. 4.— The ratio of radiative to adiabatic temperature gradients as a function of mass depth in the solar interior. The dashed line marks the location of lower boundary surface of the convection zone.

The solid curve in Figure 5 (choosing $M_{Dc} = -6.5$, $\sigma = 0.5$, $B_0 = 7$ G and $A = 190$) shows the corresponding magnetic field distribution in the solar interior in 1989, near solar maximum. Figure 6 compares the calculated (dotted curve) and measured (solid curve) cyclic irradiance variation while Figure 7 compares the calculated (dotted curve) and measured (solid curve) cyclic effective temperature variation. The irradiance fit ($\chi^2 = 3$) is better than the effective temperature fit ($\chi^2 = 43$). The computed radius variation is smaller than 4×10^{-6} , and the W parameter is almost constant, about 4×10^{-3} . Figure 8 shows the structure change generated by the field in 1989 (solid curve).

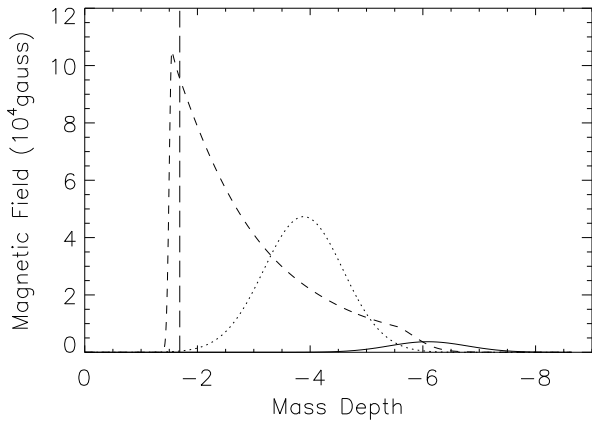


FIG. 5.— Three possible distributions of inferred magnetic field in the solar interior in 1989 according to the measured irradiance and photospheric temperature cyclic variations given in Figures 1 and 2. The vertical line indicates the base of the convection zone.

Although we can relate the magnetic field generation to the plasma turbulence in this region, the magnetic field maintenance here faces the old problem of magnetic buoyancy, as implied by Figure 4. How can we get around this problem? Observations and simulations suggest that the actual dynamics within solar convection zone is extremely intricate (Brummell et al 1995; Kim & Chan 1998; Nordlund 1999). The velocities and magnetic fields are complex, exhibiting large-scale structure and ordered behavior amidst rapidly varying and intense small-scale turbulence. In fact, the numerical simulations of the solar outer convection zone (Kim & Chan 1998; Nordlund 1999) indicate a major presence of downward moving plumes. These ordered downdrafts may gather small magnetic flux tubes generated in the extremely unstable layer to form larger flux tubes and carry them to the deeper layer. These downdrafts may also push down the magnetic flux tubes to balance the magnetic buoyancy to form a magnetized layer below the most unstable convective region.

One possibility is that these magnetic flux tubes are carried downwards into the stable subadiabatically stratified overshoot layer and then rooted and stored therein. When the stabilized force exerted on a flux tube in this layer balances the buoyancy exerted on the tube in the convection zone, the tube can partially float in the convection zone. For example, we can construct a magnetic field distribu-

tion $F = F'^3$ to mimic this case, with F' defined as follows

$$F' = \begin{cases} h(700) & M_D \geq M_{Dc} \\ h(1) - 0.325(M_D - M_{Dc}) & M_D \leq M_{Dc} \\ h(1) + 1.3 \exp[-2(M_D + 5.55)^2] & M_D \leq -5.55 \end{cases} \quad (21)$$

where $h(m) = (M_D/M_{Dc})^m \exp[-m(M_D/M_{Dc} - 1)]$. Choosing $M_{Dc} = -1.55$ in equation (21) and $B_0 = 200$ G and $A = 190$ in equation (14), we also get a good fit to Figures 1 ($\chi^2 = 4$) and 2 ($\chi^2 = 43$). The magnetic field profile is depicted as a dashed curve in Figure 4. This case is represented by dot-dashed curves in Figures 6-7 and by dashed curves in Figure 8. The predicted W parameter equals to about 2×10^{-2} . It should be noted that what contributes to the observed cycle variations of solar irradiance and effective temperature in this case is the field located within the convection zone proper and the contribution of the field confined in the overshoot layer is negligible.

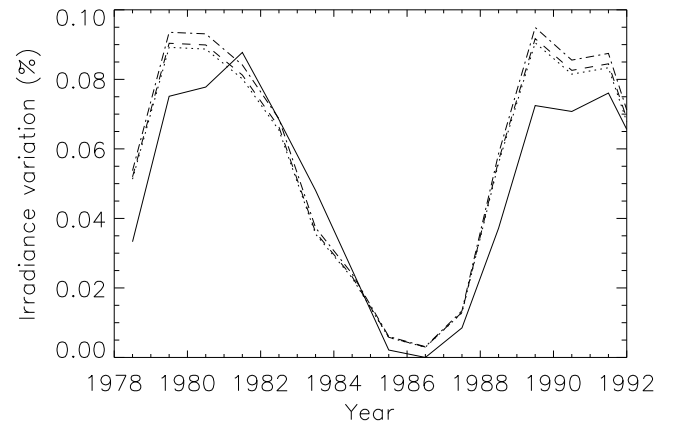


FIG. 6.— Comparison between the measured (solid curve) and calculated (dotted, dot-dashed, and dashed curves) solar irradiance variations.

Another possibility is that the downdrafts gather and carry magnetic flux tubes generated by turbulence to depths in the convective envelope until some sort of equipartition is reached. In fact, Antia, Chitre, and Thompson (2000) have explored this possibility. They employ the observed splittings of solar oscillation frequencies to separate the effects of interior solar rotation and to estimate the contribution from a large-scale magnetic field. After subtracting out the estimated contribution from rotation, there is some residual signal in the even splitting coefficients, which may be explained by a magnetic field of approximately 20 kG strength located at a depth of $M_D = -4.25$ ($r = 0.96R_\odot$) in 1996. Since the density near $M_D = -4.25$, ρ , is of 4×10^{-3} , and the downward velocity for the plumes is of order 5×10^4 cm s $^{-1}$, the estimated dynamical pressure of the plumes, ρv^2 , is equal to or larger than 10^7 dyne cm $^{-2}$, which becomes comparable with the magnetic pressure, $B^2/8\pi$, corresponding to a field strength of 20 – 30 kG. This demonstrates that a stable magnetized layer in the convection zone proper may form when the complexity of convection motion is taken into account. If we wish to reproduce the observed temperature and irradiance variations by the magnetic field at the depth indicated by helioseismology, we find that B_m ranges from 20 kG to 47 kG during a solar cycle (choosing $B_0 = 90$ G and $A = 190$), which is in good agreement with

the inference of helioseismology. Therefore, in Figures 5-8 we also show this case (dotted curves: $M_{Dc} = -4.25$, $\sigma = 0.5$). The irradiance fit ($\chi^2 = 3$) is also better than the effective temperature fit ($\chi^2 = 41$), the W parameter is equal to about 2×10^{-2} , and the predicted cyclic variation of solar radius is equal to about 2×10^{-5} , which can be tested by measuring the W parameter.

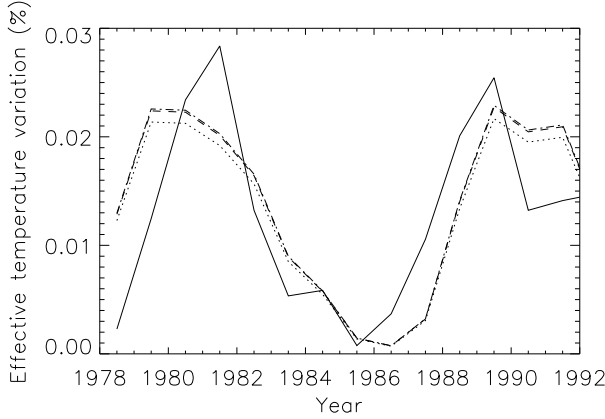


FIG. 7. — Comparison between the measured (solid curve) and calculated (dotted, dot-dashed, and dashed curves) solar photospheric temperature variations.

In fact, recent measurements carried out by the MDI experiment on SOHO have measured the W parameter. Using the data obtained between April 19, 1996 and June 24, 1998, Emilio et al (2000) find $W \leq 2 \times 10^{-2}$, which is consistent with the above prediction. This shows that the third case is in agreement with all relevant precise observations, including solar irradiance, effective temperature, radius, and p-mode oscillation observations, and so is the second case. The first case is ruled out by the measured W parameter.

5. CONCLUSIONS

It is possible to locate solar interior magnetic fields using the observed cyclic variations of three global solar parameters such as luminosity, temperature and radius at the surface of the sun, which provides an alternative probe of the solar interior magnetic fields, independent of helioseismology. Simultaneous measurements of solar total irradi-

ance and effective temperature can only select an allowed range of solar internal magnetic fields, in magnitude and location, which is consistent with helioseismic observations and recent MDI experiment on SOHO.

Although the observed cycle variations of solar irradiance, effective temperature, radius and p-mode oscillation frequencies require a magnetic field component between 20 and 47 kG peaked at $r = 0.96R_{\odot}$ within the convection zone proper, a stronger component of about 300 kG buried in the overshoot layer beneath the base of the convection zone cannot be ruled out since the contribution of the latter to those observations is negligible.

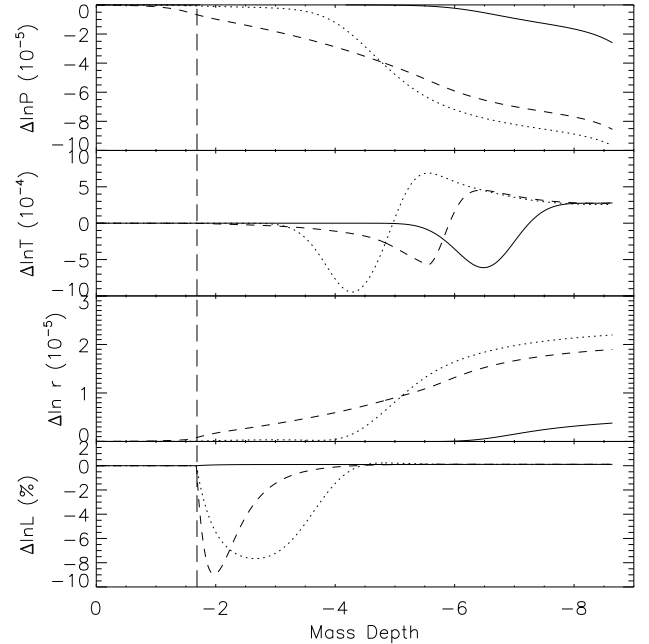


FIG. 8. — The structural changes caused by the magnetic field distributions given in Figure 5: relative pressure, temperature, radius and luminosity changes from top to bottom. The vertical line indicates the base of the convection zone.

This work was supported in part by a grant from the National Aeronautics and Space Administration, and in part by Natural Science Foundation of China (project 19675064).

REFERENCES

- Antia, H.M., Chitre, S.M., & Thompson, M.J. 2000, *A&A*, in press
 Balmforth, N.J., Gough, D.O., & Merryfield, W.J. 1996, *MNRAS*, 278, 437
 Brummell, N., Cattaneo, F. & Toomre, J. 1995, *Science*, 269, 1370
 Caligar, P., Moreno-Inertis, F. & Schüssler, M. 1995, *ApJ*, 441, 886
 Caligar, P., Moreno-Inertis, F. & Schüssler, M. 1998, *ApJ*, 502, 481
 Emilio, M., Kuhn, J.R., Bush, R.I. & Scherrer, P. 2000, *ApJ*, in press
 Endal, A.S., Sofia, S. & Twigg, L.W. 1985, *ApJ*, 290, 748
 Fröhlich, C. & Lean, J. 1998, in *IAU Symposium 185: New Eyes to See Inside the Sun and Stars*, ed. F.L. Deubner, (Dortrecht: Kluwer Academic Publ.), 89
 Gray, D.F. & Livingston, W.C. 1997a, *ApJ*, 474, 798
 Gray, D.F. & Livingston, W.C. 1997b, *ApJ*, 474, 802
 Guenther, D.B., Demarque, P., Kim, Y.-C., and Pinsonneault, M.H. 1992, *ApJ*, 387, 372
 Kim, Y.-C. & K.L., Chan 1998, *ApJ*, 496, L121
 Kippenhahn, R. & Weigert, A. 1990, *Stellar Structure and Evolution* (Berlin: Springer-Verlag).
 Lean, J.L., Cook, J., Marquette, W. & Johannesson, A. 1998, *ApJ*, 492, 390
 Libbrecht, K.G. & Woodard, M.F. 1990, *Nature*, 345, 779
 Lydon, T.J. & Sofia, S. 1995, *ApJS*, 101, 357
 Lydon, T.J., Guenther, D.B. & Sofia, S. 1996, *ApJ*, 456, L127
 Nordlund, Å 1999, *IAU Colloquium 179 on Cyclical evolution of solar magnetic fields: Advances in theory and observations*.
 Prather, M.J. 1976, Ph.D. dissertation, Yale University.
 Willson, R.C. & Hudson, H.S. 1991, *Nature*, 351, 42